Tension Force Estimation of Cables with two Intermediate supports

Banfu Yan[1], Wenbing Chen[2], You Dong[*3], and Xiaomo Jiang[4]

Abstract:

The presence of intermediate supports usually imposes difficulties in identifying the tension force of stayed cables in cable-stayed bridges or hanger cables in arch bridges. This paper establishes the partial differential equations of motion of the cable and derives two numerical models with (Model 1) and without (Model 2) considering the flexural rigidity. The effects of two intermediate supports on the identification accuracy of the cable tension force are further studied analytically and experimentally. The effects of several non-dimensional parameters (e.g., damper location, support stiffness, flexural rigidity, and mode order of the cable) on the identification accuracy of the models are also investigated. It is theoretically concluded that the simplified Model 2 provides acceptable accuracy on tension force identification when the non-dimensional parameter ξ is greater than 90 (slender cables), while the accurate Model 1 can be applied for tension force identification at any scenarios. The feasibility of two models is further verified by three numerical examples and field tests on two real-world arch bridges.

Key words: Cable; Tension force estimation; Field test; Intermediate support; Flexural rigidity; Cable-stayed bridge; Arch bridge

---

[1] Associate Professor, College of Civil Engineering, Hunan University, Yuelushan, Changsha, Hunan 410082, P.R. China; Key Laboratory for Wind and Bridge Engineering of Hunan Province, Changsha 410082, Hunan, China; E-mail: yanbanfu@hnu.edu.cn ;
[2] Ph.D Candidate, College of Civil Engineering, Hunan University, Yuelushan, Changsha, Hunan 410082, P.R. China; E-mail: cwb1993@hnu.edu.cn ;
[3,*] Assistant Professor, Department of Civil and Environmental Engineering, The HONG KONG Polytechnic University, Hong hum, HONG KONG, China. E-mail: you.dong@polyu.edu.hk ; corresponding author;
[4] Visiting Professor, College of Civil Engineering, Hunan University, Yulushan, Changsha, Hunan 410082, P.R. China; E-mail: xiaomojiang2017@163.com

1. INTRODUCTION

Accurate estimation of the tension force of stay cable for cable stayed bridge or the axial force within hanger cables of half-through or through arch bridge plays an important role on overall condition assessment of a bridge during its construction stage and service life. Instead of the direct measurement methods (e.g., jack hydraulic method and force transducer), the vibration-based method is employed to identify the natural frequency of the cable from its dynamic response signals under ambient or artificial excitations. A cable vibration model is then established to estimate the cable force through the relationship between the measured natural frequencies and the tension force.[1, 2] For a cable with purely pinned-pinned or clamped-clamped conditions, multiple models have been developed to establish the relationship between the cable force and the measured natural frequencies in the form of empirical explicit expression, approximate formulation, and iterative solution.[3-5] For a cable with two arbitrary end conditions, a tensioned beam model with arbitrary supporting stiffness and rotational stiffness would be constructed and then the frequency equation can be established.[6] The tension force can be determined by solving a very complicated transcendental equation in an iterative way. Kim and Park[7] developed a frequency-based sensitivity-updating algorithm to determine the tensile force of a cable, based on measured multi-order natural vibration frequencies and a finite element model considering the bending stiffness and the sag effect of the cable. Ma[8] proposed an inclined cable model considering the unknown rotational constraint stiffness at both ends of the cable. A numerical approach was then employed to obtain the cable tension, the flexural rigidity and the rotational stiffness at the cable ends by iterative updating. These studies indicate that, in some sense, the tension force of a cable with two arbitrary end conditions is readily obtained numerically.

For the existing in-service bridges, the intermediate supports, such as the internal or external dampers installed at the cable ends near to the deck and pylon, divide the cable into two or three segments. In such cases, the boundary conditions of the cable are complicated that it is difficult to construct the relationship between the cable force and the measured natural frequencies via the general dynamic model. For a cable with one or two intermediate supports, many studies[9-19] investigated the vibration characteristics of the cable-damper systems by solving the differential equations of the free lateral vibrations of the cable. However, these studies were conducted from the viewpoint of the damper design rather than focusing on the cable force estimation.

From the view of cable force identification, an empirical approach was proposed to determine the equivalent vibration length of the cable by measuring the variations of natural frequencies before and after the installation of the dampers. This approach, however, is impractical to remove the intermediate cable supports for in-service bridges. Consequently, the limitation of the vibration method in dealing with the intermediate supports needs to be carefully taken into account. Ceballos and Prato[20] simplified the intermediate supports near the anchors as deviators having no own rotational stiffness and restraining the transversal displacement only. Chen *et al.*[21, 22] proposed a method to combine the mode shape ratios with the modal frequencies in order to determine stay cable forces. Yan *et al.*[23] transformed the cable force estimation problem into finding the zero-amplitude points from the mode shape of the cable. Their methods can eliminate the effects of complex boundary conditions. However, application of this method to practical field test requires accurate identification of the mode shape. The conventional ambient vibration-based measurement system generally requires installing numerous contact-type sensors, such as accelerometers or velocimeters. These sensors are attached to the cable in order to obtain the

observable mode shapes, which appears to be very difficult and even impossible within construction stage and operational state. As stated by Yan *et al.*[24], one of the possible solutions is to integrate the vision-based measurement for the multiple specific ranges of the cable with the automatic total station for target positioning, with the purpose of detecting the zero-amplitude points from the identified local mode shapes.

In practical engineering, the compressive-type high damping rubber (HDR) dampers as the internal dampers protected by the steel tube near the deck and pylon anchorage zones are commonly introduced to the cable. Generally, the cable force is not very sensitive to the supporting stiffness of the HDR damper attached to the cable, hence, its supporting stiffness can be directly determined from the technical specification of the HDR damper. The stiffness variation resulted from the installation deviation of the damper can be neglected. This paper establishes an in-plane cable-double damping model (Model 1) for a tensioned cable with two known intermediate supporting stiffness values. The objective of this paper is to study the effect of these two intermediate supports on the tension force estimation of the cable. The analytical solution is obtained by introducing the boundary equation and continuity condition. By constructing different parameters, the proposed Model 1 is compared with the cable-double damping model (Model 2) without considering the flexural rigidity. The effectiveness of the model is verified by a simulation example for three typical cables and two field tests on the tension force identification of the hanger cable for two arch bridges.

2. Dynamics of A Cable with Two Dampers

2.1 Model 1: Considering flexural rigidity of the cable

A clamped-clamped cable with two intermediate compression-type high damping rubber (HDR) dampers is shown in Fig. 1. The cable has the cable force T along the chord, the mass per unit length m, the chord length L, and the flexural rigidity EI. For the small deflection, the differential equation of the free lateral vibrations for the cable with a uniform cross section can be written as:

$$EI\frac{\partial^4 v(x,t)}{\partial x^4}-T\frac{\partial^2 v(x,t)}{\partial x^2}+m\frac{\partial^2 v(x,t)}{\partial t^2}=f_1(t)\delta(x-x_1)+f_2(t)\delta(x-x_2) \tag{1}$$

where x is the coordinate along the cable chord, $v(x,t)$ is the transverse displacement at time t, $f_1(t)$ and $f_2(t)$ are the damping forces at time t for two dampers with supporting stiffness k_1 and k_2, respectively, which are located at the distances of x_1 and x_2 from the left ends, respectively, and $\delta(\cdot)$ is the Dirac delta function, specifying the locations of the damper forces at $x=x_1$ and $x=x_2$. To simplify the calculation, the sag of the cable is neglected in the model.

The compressive-type HDR dampers can be simplified into a spring element with compression stiffness of $k_i=E_iA_i/t_i$ $(i=1,\ 2)$, where E_i is the elastic modulus of the rubber, A_i is the contact area of the cable with the HDR, and t_i is the thickness of the rubber.

For the free vibration of the cable, the transverse vibration displacement and the damping force can be described as follows:

$$v(x,t)=\tilde{v}(x)e^{i\omega t} \tag{2}$$

$$f_j(t)=F_je^{i\omega t}\ (j=1,2) \tag{3}$$

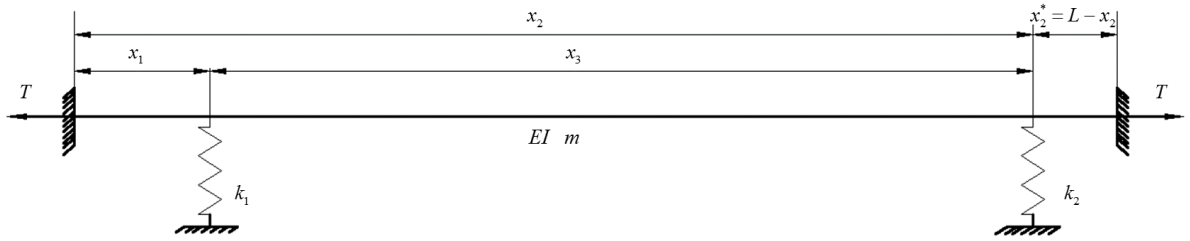

Fig. 1. Model 1: cable with two attached HDR dampers ($EI\neq 0$)

where $i^2=-1$, ω is the circular frequency of the free vibration of the cable, and $\tilde{v}(x)$ is the complex mode shape. Substituting Eqs. (2) and (3) into Eq. (1), a fourth-order ordinary differential equation is obtained in the form of

$$EI\frac{d^4\tilde{v}(x)}{dx^4}-T\frac{d^2\tilde{v}(x)}{dx^2}-m\omega^2\tilde{v}(x)=0 \tag{4}$$

which can be iteratively solved through classical procedures. The mode shape of the cable can be written in the non-dimensional form as

$$\tilde{v}(\varepsilon)=D_1\sin(\hat{\alpha}\varepsilon)+D_2\cos(\hat{\alpha}\varepsilon)+D_3\sinh(\hat{\beta}\varepsilon)+D_4\cosh(\hat{\beta}\varepsilon) \tag{5}$$

where D_i $(i=1,\ 2,\ 3,\ 4)$ is the undetermined coefficient, $\varepsilon=x/L$ $(0\le x\le L)$ is the strain, and

$$\hat{\alpha}=\alpha L=\frac{\xi}{\sqrt{2}}\sqrt{\sqrt{1+\left(\frac{2n\pi\eta_n}{\xi}\right)^2}-1} \tag{6a}$$

$$\hat{\beta}=\beta L=\frac{\xi}{\sqrt{2}}\sqrt{\sqrt{1+\left(\frac{2n\pi\eta_n}{\xi}\right)^2}+1} \tag{6b}$$

in which

$$\xi=L\sqrt{\frac{T}{EI}},\quad \eta_n=\frac{\omega_n L}{n\pi}\sqrt{\frac{m}{T}} \tag{6c}$$

where ω_n is the nth circular frequency of the cable, ξ .and η_n are two non-dimensional parameters.

As shown in Fig. 1, the cable is divided into three segments, i.e. the left span ($0\le x\le x_1$), the intermediate span ($x_1\le x\le x_2$), and the right span ($x_2\le x\le L$) of the cable. The displacements and slopes at the left and right ends of the cable with fixed constraints are equal to zero, i.e. $\tilde{v}_1(0)=\tilde{v}_1'(0)=0$ and $\tilde{v}_3(0)=\tilde{v}_3'(0)=0$. The mode shapes at the left span, the intermediate span and the right span are respectively given by

$$\begin{cases} v_1(\varepsilon) = A_1\left[\cos\left(\hat{\alpha}\varepsilon\right) - \cosh\left(\hat{\beta}\varepsilon\right)\right] + A_2\left[\sin\left(\hat{\alpha}\varepsilon\right) - \hat{\alpha}\sinh\left(\hat{\beta}\varepsilon\right)/\hat{\beta}\right] & 0 \le \varepsilon \le \varepsilon_1 \\ v_2(\varepsilon') = A_3\cos(\hat{\alpha}\varepsilon') + A_4\sin(\hat{\alpha}\varepsilon') + A_5\cosh(\hat{\beta}\varepsilon') + A_6\sinh(\hat{\beta}\varepsilon') & 0 \le \varepsilon' \le \varepsilon_3 \\ v_3(\varepsilon^*) = A_7\left[\cos\left(\hat{\alpha}\varepsilon^*\right) - \cosh\left(\hat{\beta}\varepsilon^*\right)\right] + A_8\left[\sin\left(\hat{\alpha}\varepsilon^*\right) - \hat{\alpha}\sinh\left(\hat{\beta}\varepsilon^*\right)/\hat{\beta}\right] & 0 \le \varepsilon^* \le \varepsilon_2^* \end{cases} \tag{7}$$

where $\varepsilon_1 = x_1/L$, $\varepsilon_3 = x_3/L = (x_2 - x_1)/L$, and $\varepsilon_2^* = (L - x_2)/L = x_2^*$.

The boundary and continuity conditions of the cable at the locations of the damper $x = x_1$ and $x = x_2$ can be expressed, respectively, as follows

$$\tilde{v}_1(\varepsilon_1) = \tilde{v}_2(0) \qquad \tilde{v}_1'(\varepsilon_1) = \tilde{v}_2'(0) \qquad \tilde{v}_1''(\varepsilon_1) = \tilde{v}_2''(0) \tag{8a}$$

$$\tilde{v}_2(\varepsilon_3) = \tilde{v}_3(\varepsilon_2^*) \qquad \tilde{v}_2'(\varepsilon_3) = \tilde{v}_3'(\varepsilon_2^*) \qquad \tilde{v}_2''(\varepsilon_3) = \tilde{v}_3''(\varepsilon_2^*) \tag{8b}$$

and

$$EI(\tilde{v}_2'''(0) - \tilde{v}_1'''(\varepsilon_1)) = -F_1 \qquad EI(\tilde{v}_3'''(\varepsilon_2^*) - \tilde{v}_2'''(\varepsilon_3)) = -F_2 \tag{8c}$$

The displacements of the cable at the locations of two dampers can be expressed in the forms of $\tilde{v}_1(\varepsilon_1) = \tilde{v}_2(0) = \tilde{v}_{11}$ and $\tilde{v}_2(\varepsilon_3) = \tilde{v}_3(\varepsilon_2^*) = \tilde{v}_{22}$, thus, Eq. (7) can be rewritten in the form of

$$DA = S \tag{9}$$

where $S = (0,0,0,v_{11},0,0,0,v_{22})^T$, $A = (A_1, A_2, \cdots, A_7, A_8)^T$, and

$$D = \begin{bmatrix} C_1 - CH_1 & S_1 - \hat{\alpha}SH_1/\hat{\beta} & -1 & 0 & -1 & 0 & 0 & 0 \\ -\hat{\alpha}S_1 - \hat{\beta}SH_1 & \hat{\alpha}C_1 - \hat{\alpha}CH_1 & 0 & -1 & 0 & -1 & 0 & 0 \\ -\hat{\alpha}^2C_1 - \hat{\beta}^2CH_1 & -\hat{\alpha}^2S_1 - \hat{\alpha}\hat{\beta}SH_1 & \hat{\alpha}^2 & 0 & -\hat{\beta}^2 & 0 & 0 & 0 \\ 0 & 0 & 1 & 0 & 1 & 0 & 0 & 0 \\ 0 & 0 & C_3 & S_3 & CH_3 & SH_3 & -C_2^* + CH_2^* & -S_2^* + \hat{\alpha}SH_2^*/\hat{\beta} \\ 0 & 0 & -\hat{\alpha}S_3 & \hat{\alpha}C_3 & \hat{\beta}SH_3 & \hat{\beta}CH_3 & -\hat{\alpha}S_2^* - \hat{\beta}SH_2^* & \hat{\alpha}C_2^* - CH_2^* \\ 0 & 0 & -\hat{\alpha}^2C_3 & -\hat{\alpha}^2S_3 & \hat{\beta}^2CH_3 & \hat{\beta}^2SH_3 & \hat{\alpha}^2CH_2^* + \hat{\beta}^2CH_2^* & \hat{\alpha}^2S_2^* + \hat{\alpha}\hat{\beta}SH_2^* \\ 0 & 0 & 0 & 0 & 0 & 0 & C_2^* - CH_2^* & S_2^* - \hat{\alpha}SH_2^*/\hat{\beta} \end{bmatrix} \tag{10}$$

in which $C_i = \cos(\hat{\alpha}\varepsilon_i)$, $CH_i = \cosh(\hat{\beta}\varepsilon_i)$, $S_i = \sin(\hat{\alpha}\varepsilon_i)$, $SH_i = \sinh(\hat{\beta}\varepsilon_i)$ $(i = 1\sim3)$, $C_2^* = \cos(\hat{\alpha}\varepsilon_2^*)$, $CH_2^* = \cosh(\hat{\beta}\varepsilon_2^*)$, $S_2^* = \sin(\hat{\alpha}\varepsilon_2^*)$, and $SH_2^* = \sinh(\hat{\beta}\varepsilon_2^*)$

In Eq. (9), let

$$A_i = (M_i v_{11} + N_i v_{22}) \qquad (i = 1\sim8) \tag{11}$$

where M_i and N_i $(i=1\sim8)$ are the combinations of trigonometric functions and hyperbolic functions, which can be obtained through solving the system of first order equations of Eq. (9) with eight variables. Based on the continuity conditions of Eqs. (8a) ~ (8b) and substituting the constants A_i $(i=1,2,...,8)$ into Eq. (8c), two formulas can be obtained

$$\begin{aligned}&-\hat{\alpha}^3A_4+\hat{\beta}^3A_6-A_1(\hat{\alpha}^3\sin(\hat{\alpha}\varepsilon_1)-\hat{\beta}^3\sinh(\hat{\beta}\varepsilon_1))\\&-A_2(-\hat{\alpha}^3\cos(\hat{\alpha}\varepsilon_1)-\hat{\alpha}\hat{\beta}^2\cosh(\hat{\beta}\varepsilon_1))=-\frac{F_1L^3}{EI}\end{aligned}\tag{12.a}$$

$$\begin{aligned}&-A_7(\hat{\alpha}^3\sin(\hat{\alpha}\varepsilon_2^*)-\hat{\beta}^3\sinh(\hat{\beta}\varepsilon_2^*))-A_8(-\hat{\alpha}^3\cos(\hat{\alpha}\varepsilon_2^*)-\hat{\alpha}\beta^2\cosh(\hat{\beta}\varepsilon_2^*))\\&-\hat{\alpha}^3A_3\sin(\hat{\alpha}\varepsilon_3)+\hat{\alpha}^3A_4\cos(\hat{\alpha}\varepsilon_3)+\hat{\beta}^3A_5\sinh(\hat{\beta}\varepsilon_3)-\hat{\beta}^3A_6\cosh(\hat{\beta}\varepsilon_3)=-\frac{F_2L^3}{EI}\end{aligned}\tag{12.b}$$

Substituting Eq. (11) into Eqs. (12.a) and (12.b) with the non-dimensional parameters of

$$K_{11}=\frac{F_1L^3}{EIv_{11}}=\frac{k_1L^3}{EI},\quad K_{12}=\frac{F_2L^3}{EIv_{22}}=\frac{k_2L^3}{EI}\tag{13}$$

We can obtain the frequency equation of the cable as follows:

$$\begin{aligned}&-(M_7Z+N_7)(\hat{\alpha}^3\sin(\hat{\alpha}\varepsilon_2^*)-\hat{\beta}^3\sinh(\hat{\beta}\varepsilon_2^*))-(M_8Z+N_8)(-\hat{\alpha}^3\cos(\hat{\alpha}\varepsilon_2^*)-\hat{\alpha}\beta^2\cosh(\hat{\beta}\varepsilon_2^*))\\&-\hat{\alpha}^3(M_3Z+N_3)\sin(\hat{\alpha}\varepsilon_3)+\hat{\alpha}^3(M_4Z+N_4)\cos(\hat{\alpha}\varepsilon_3)+\hat{\beta}^3(M_5Z+N_5)\sinh(\hat{\beta}\varepsilon_3)\\&-\hat{\beta}^3(M_6Z+N_6)\cosh(\hat{\beta}\varepsilon_3)+K_{12}=0\end{aligned}\tag{14.a}$$

where

$$Z=\frac{N_2[-\hat{\alpha}^3\cos(\hat{\alpha}\varepsilon_1)-\hat{\alpha}\hat{\beta}^2\cosh(\hat{\beta}\varepsilon_1))+\hat{\alpha}^3N_4-\hat{\beta}^3N_6+N_1(\hat{\alpha}^3\sin(\hat{\alpha}\varepsilon_1)+\hat{\beta}^3\sinh(\hat{\beta}\varepsilon_1)]}{K_{11}+M_2[\hat{\alpha}^3\cos(\hat{\alpha}^3\varepsilon_1)+\hat{\alpha}\hat{\beta}^2\cosh(\hat{\beta}\varepsilon_1))-\hat{\alpha}^3M_4+\hat{\beta}^3M_6-M_1(\hat{\alpha}^3\sin(\hat{\alpha}\varepsilon_1)-\hat{\beta}^3\sinh(\hat{\beta}\varepsilon_1)]}\tag{14.b}$$

The frequency equation is an implicit transcendental equation, and the unknown parameter η_n is generally solved by the iterative method. Generally, it is difficult to obtain parameter η_n by using the common iterative method due to the complexity of the transcendental equation. Dan *et al*. (2014) investigated numerical solutions by integrating interval solution method and Newton-Raphson for nonlinear frequency equations. Herein, we integrate the interval solution based on the image of the frequency equation and the dichotomy procedures to solve the nonlinear

frequency equation.

The implicit frequency Eq. (14.a) can be written in the form of $f(\eta_n) = 0$, and its solution is associated with the zero root. As indicated in Fig. 2, we display the relationship of $f(\eta_n)$ and η_n in the form of an image, from which the resolving interval covering the zero root can be determined. Note that there are two break points in the image of $f(\eta_n) \sim \eta_n$. As indicated, there exists a zero root between these two break points in region "b", which however is a false solution. In the study, it is necessary to determine the appropriate solution interval, where a correct zero root can be found from the image of $f(\eta_n) \sim \eta_n$. The region "a" covering one zero point is selected as the interval of the initial solution, and the dichotomy method is then employed to find the approxiamate solution of the frequency equation with a certain degree of accuracy.

Once the parameter η_n is attained, the tension force can be estimated as follows:

$$T = \frac{m\omega_n^2 L^2}{n^2 \pi^2 \eta_n^2} \tag{15}$$

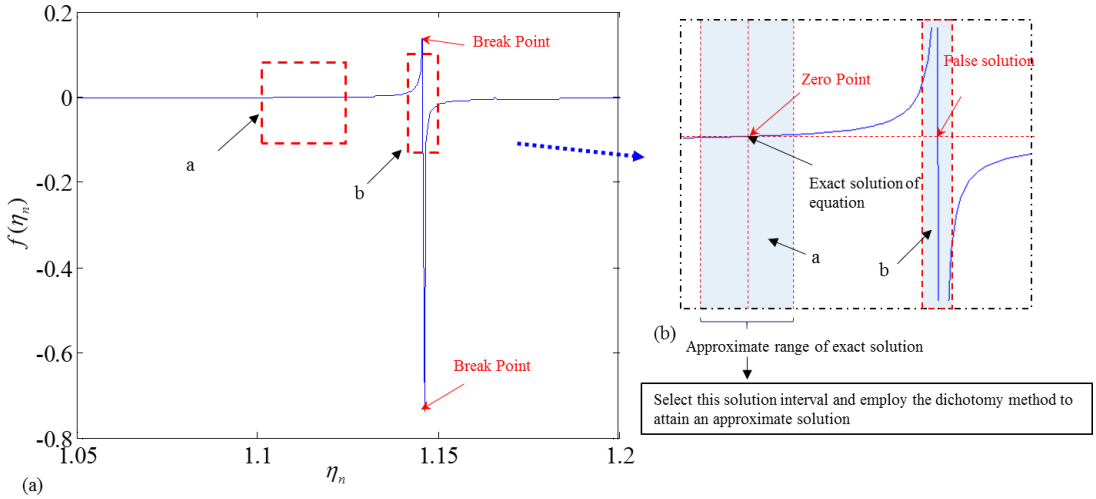

Fig. 2. (a) image of $f(\eta_n) \sim \eta_n$ and (b) selection of solution interval with zero root

2.2 Model 2: without considering flexural rigidity of the cable

For comparison purpose, a tensioned cable with two transversely attached intermediate supports shown in Fig. 3 is created. The cable has the cable force T along the chord, the mass per unit length m, and the chord length L. The sag and flexural rigidity of the cable are neglected for sake of simplicity. The differential equation of in-plane motion of the cable can be written as

$$-T\frac{\partial^2 v}{\partial x^2}+m\frac{\partial^2 v}{\partial t^2}=f_1(t)\delta(x-x_1)+f_2(t)\delta(x-x_2) \tag{16}$$

According to the derivation process[14], with the boundary and continuity conditions of the cable at the damper locations, the frequency equation of the cable is given as:

$$\tan\hat{\beta}=\frac{\frac{K_{21}}{\hat{\beta}}\sin^2\hat{\beta}\varepsilon_1+\frac{K_{22}}{\hat{\beta}}\sin^2\hat{\beta}\varepsilon_2^*+\frac{K_{21}}{\hat{\beta}}\frac{K_{22}}{\hat{\beta}}\sin\hat{\beta}\varepsilon_1\sin\hat{\beta}\varepsilon_2^*\sin\hat{\beta}\left(\varepsilon_1+\varepsilon_2^*\right)}{1+\frac{K_{21}}{\hat{\beta}}\sin\hat{\beta}\varepsilon_1\cos\hat{\beta}\varepsilon_1+\frac{K_{22}}{\hat{\beta}}\sin\hat{\beta}\varepsilon_2^*\cos\hat{\beta}\varepsilon_2^*+\frac{K_{21}}{\hat{\beta}}\frac{K_{22}}{\hat{\beta}}\sin\hat{\beta}\varepsilon_1\sin\hat{\beta}\varepsilon_2^*\cos\hat{\beta}\left(\varepsilon_1+\varepsilon_2^*\right)} \tag{17}$$

where $\varepsilon_1=x_1/L$ and $\varepsilon_2^*=(L-x_2)/L=x_2^*$ are the non-dimensional position of the supports, and $\hat{\beta}=\beta L=\omega_n L\sqrt{m/T}$ is the wave number. The non-dimensional parameters $K_{21}=k_1L/T$ and $K_{22}=k_2L/T$ are the supporting stiffness values of the compression-type HDR dampers at two ends.

Considering that the intermediate supports are located very close to the ends, i.e., ε_1 and ε_2^* are very small. Equation (17) can be rewritten in a simpler asymptotic expression. As the simplification inevitably introduces errors, the solution $\hat{\beta}_n$ is further improved based on Eq. (17)

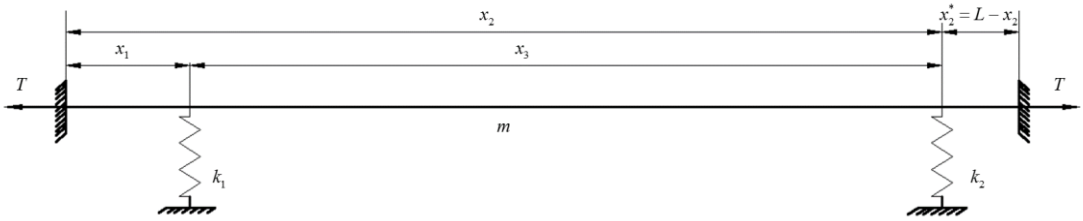

Fig. 3. Mode 2: Cable with two attached HDR supports ($EI=0$)

via the general iterative method with the initial value of $\hat{\beta}_n^0=n\pi$ (n is the mode order). The tension force of the cable can then be obtained as

$$T=\frac{m\omega_n^2L^2}{\hat{\beta}_n^2} \tag{18}$$

3. Parametric study on Model 1 and Model 2

The above derivation for Model 1 indicates that, considering the flexural rigidity of the cable, the frequency equation is very complex as shown in Eq. (14). In practical engineering, when the flexural rigidity of the cable is not very large, a relatively simple expression based on Model 2 (Equation 18) with acceptable identification accuracy can be used to reduce the calculation cost. Moreover, the range of the parameter ξ for the general cable is very large. For a short cable with relatively large flexural rigidity, Model 1 with the higher identification accuracy is still needed to establish the relationship between the measured natural frequency and the cable tension force. This section investigates the effect of the non-dimensional parameters of ε, K, and ξ on the frequency ratio η_n, from which the tension force can be estimated.

Fig. 4 shows the variation of frequency ratio η with respect to the non-dimensional parameters K (=10^0~10^{10}, K_1=K_2), and ξ (=0~200) at six different intermediate supports locations, i.e. (a) $\varepsilon_1=\varepsilon_2^*=0.02$; (b) $\varepsilon_1=\varepsilon_2^*=0.04$; (c) $\varepsilon_1=\varepsilon_2^*=0.06$; (d) $\varepsilon_1=\varepsilon_2^*=0.08$; (e) $\varepsilon_1=\varepsilon_2^*=0.10$; and (f) $\varepsilon_1=\varepsilon_2^*=0.12$. The mode order considered is the fundamental frequency ($n=1$). Fig. 5 shows the influences of ε and ξ on η in the cases of (a) $K=10^3$; (b) $K=10^5$; (c) $K=10^7$, and (d) $K=10^9$. Several observations are drawn as follows. First, no matter what kinds of intermediate supports are introduced, the relationship between the frequency ratio η

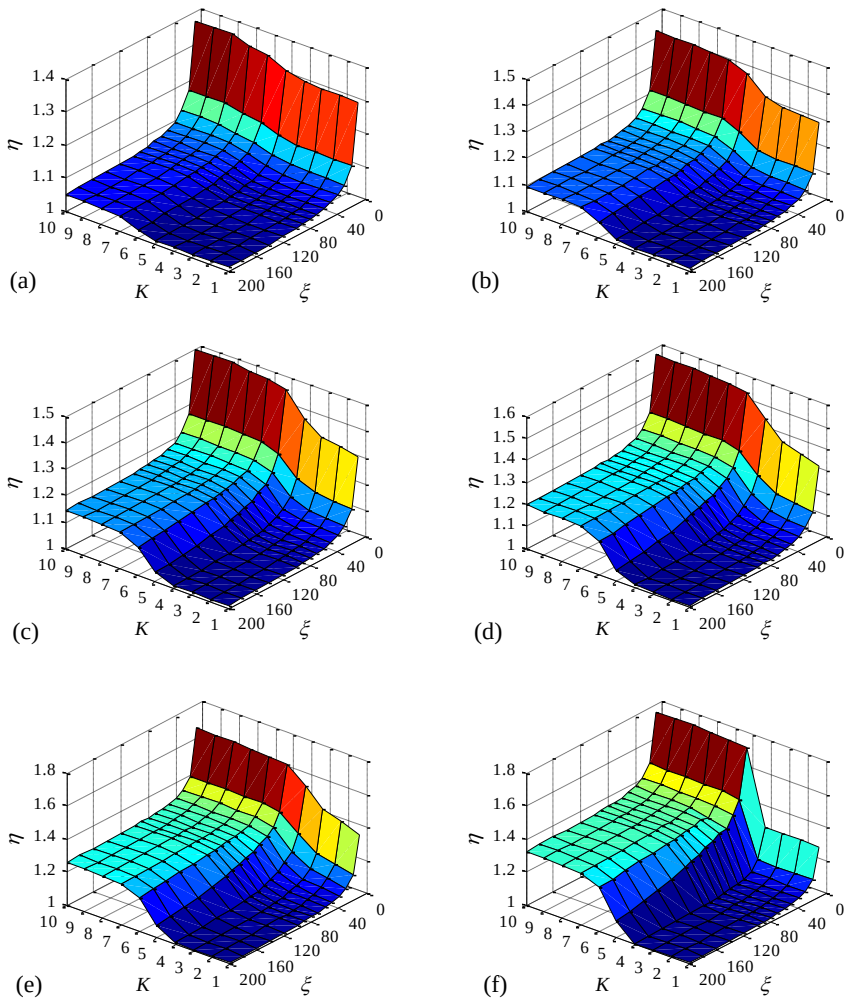

Fig. 4. Influences of K and ξ on η in the cases of (a) $\varepsilon_1 = \varepsilon_2^* = 0.02$; (b) $\varepsilon_1 = \varepsilon_2^* = 0.04$; (c) $\varepsilon_1 = \varepsilon_2^* = 0.06$; (d) $\varepsilon_1 = \varepsilon_2^* = 0.08$; (e) $\varepsilon_1 = \varepsilon_2^* = 0.10$, and (f) $\varepsilon_1 = \varepsilon_2^* = 0.12$

and the parameter ξ is approximately exponential. The parameter η increases with the decrease of ξ. In the range of $\xi = 0 \sim 60$, the parameter η appears to decrease rapidly. Whereas in the range of $\xi = 60 \sim 200$, it decreases gradually. Consequently, the presence of the flexural rigidity of the short cable should be considered carefully in estimation of cable force.

Second, the effect of the non-dimensional support stiffness K on η is in the form of "Z"-shape. In the case of $K < 10^3$ and $K > 10^8$, η increases very slowly with the increasing of K. The effect of intermediate supports on the cable is insignificant when $K < 10^3$, whereas the

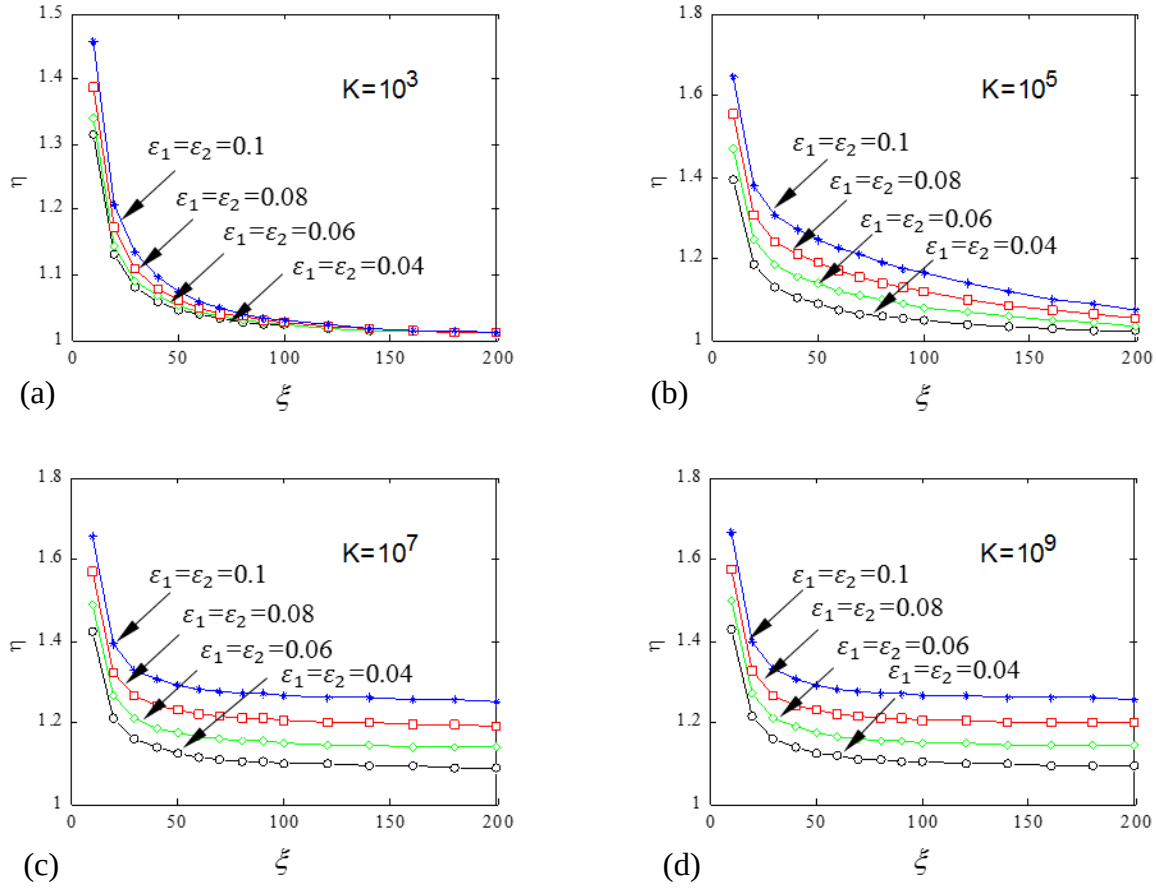

Fig. 5. Influences of ε and ξ on η in the cases of (a) $K=10^3$; (b) $K=10^5$; (c) $K=10^7$; (d) $K=10^9$

intermediate supports can be regarded as fixed ends when $K>10^8$. Moreover, in the case of $10^3<K<10^8$, the relationship between η and K is approximately in the form of linear increase.

Third, the frequency ratio η increases gradually with the increase of ε as the effective length of the cable is shortened, and its overall flexural rigidity increases due to the introduction of intermediate supports. Forth and the last, the weak constraint of the intermediate support (for instance $K<10^3$) results in the weak influence of its location ε on η. Especially in the case of $\xi \geq 60$ and $K=10^3$ with different values of ε from 0.04 to 0.1, the curve η-ξ tends to be identical. With the increase of K, as shown in Fig. 5(b)-(d), the η-ξ curves under different support locations ε (i.e., 0.04, 0.06, 0.08, and 0.10) indicate significant differences which can

be easily distinguished.

4 Relative error analysis

This section investigates the relative error from Model 2 when used in the practical engineering. The relative error ρ between Model 1 and Model 2 is defined as

$$\rho=\frac{T_2-T_1}{T_1}\cdot 100\% \tag{19}$$

where T_1 and T_2 are the tension forces calculated according to Model 1 and Model 2, respectively. The value T_1 is assumed as the exact value since the effect of flexural rigidity of the cable is considered in Model 1.

4.1 Influences of ξ, K and ε

The estimation of the cable force is largely affected by the non-dimensional bending stiffness parameter ξ, the supporting stiffness K and the location of the intermediate support ε. Note that the definitions on the dimensionless damper supporting stiffness are kL^3/EI for Model 1 and kL/T for Model 2. To avoid confusion, the same supporting stiffness k is used for Model 1 and Model 2, and $K=kL^3/EI$ is employed for further parametric analysis. For a given K, we generally substitute $k=KEI/L^3$ into kL/T to obtain K/ξ^2 for Model 2.

Fig. 6 shows the influences of ε and ξ on ρ in the cases of: (a) $\varepsilon_1=\varepsilon_2^*=0.04$; (b) $\varepsilon_1=\varepsilon_2^*=0.06$; (c) $\varepsilon_1=\varepsilon_2^*=0.08$, and (d) $\varepsilon_1=\varepsilon_2^*=0.10$. The mode order considered is the fundamental frequency ($n=1$). Three observations are drawn from Fig. 6. First, among these three parameters, ξ has the greatest influence on the relative error ρ. When $\xi\le 10$, the relative error ρ between the two models reaches about 80%; When $\xi\ge 60$, the trend of the ρ-ξ curve becomes

flat; When $\xi \geq 90$, the relative error ρ is less than 5%, which would be attributed to the damper support stiffness K and the support installation position ε.

Second, when ξ and ε are constant, the relative error ρ has the minimum value around $K = 10^5$ and the maximum value around $K = 10^3$. The relative error ρ increases when K is far larger than these values, which can also be observed from Fig. 6. Third and last, the specific application scope of Model 2 can be obtained through the parameter analysis. In the case of $\xi \geq 90$, the accuracy of Model 2 meets the requirement of $\rho \leq 0.05$ regardless of the other two parameters K and ε. Note that K has significant effect on ρ for a given ξ and ε. The

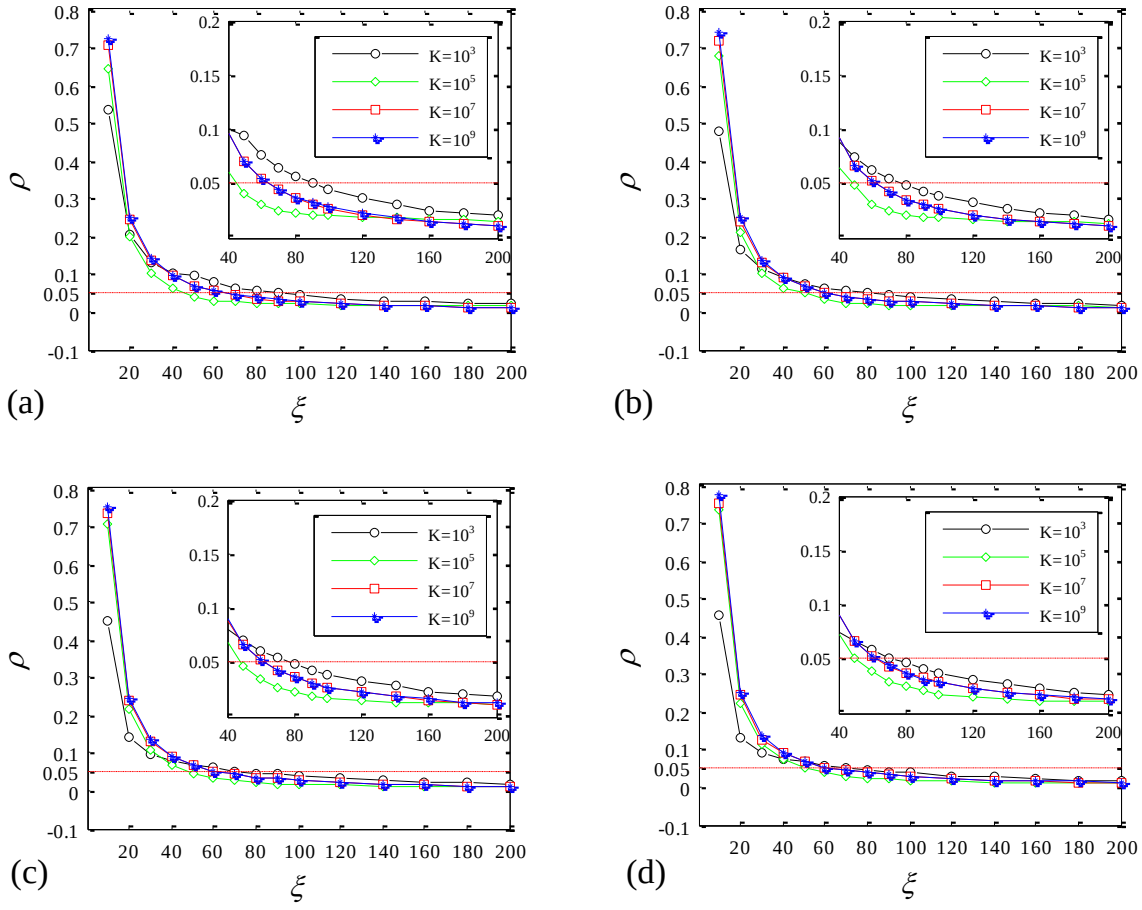

Fig. 6. Influences of K and ξ on ρ in the cases of: (a) $\varepsilon_1 = \varepsilon_2^* = 0.04$; (b) $\varepsilon_1 = \varepsilon_2^* = 0.06$; (c) $\varepsilon_1 = \varepsilon_2^* = 0.08$; (d) $\varepsilon_1 = \varepsilon_2^* = 0.10$

accuracy ρ attains its minimum value when $K=10^5$. In such case, ξ can be set to be larger than 50.

4.2 Influence of modal order

Note that the mode order considered in section 4.1 is the fundamental frequency ($n=1$). In practical engineering, due to the presence of the intermediate supports and the flexural rigidity of the cable, the high-order frequency and the fundamental frequency are no longer simple linear relationship, which indicates that the influence of each mode order on the relative error is different. Hence, the mode order number *n* should be carefully considered in error analysis. Fig. 7 shows the effects of the mode order *n* on the frequency ratio η and the relative error ρ between two models in the cases of (a) and (b): $\xi=30$; (c) and (d): $\xi=80$; (e) and (f): $\xi=110$ when $\varepsilon_1=\varepsilon_2=0.06$. It is observed that when the parameter ξ is small, the effects of the different mode order *n* on the frequency ratio η and the relative error ρ between the two models are quite different. With the increase of ξ, the difference gradually becomes the smaller. The larger the mode order, the larger the frequency ratio and the relative error of between two models. Particularly in the case of $n=1$ and $\xi=80$, no matter how K changes, the relative error is smaller than 5%. Whereas in the case of $\xi=110$, for the first and second mode orders, the relative error is always smaller than 5% no matter how K changes. Hence it is desirable to estimate the tension force of the cable using its first mode frequency.

5. Numerical analysis

Three typical cables are used to verify the effectiveness of the formulas derived from Model 1 and Model 2. Table 1 presents the basic parameters of the three cables. The dimensionless bending stiffness ξ of these three cables is set to be 59.74, 95.58 and 119.48, respectively. The support stiffness K of these two intermediate supports are identical, varying from 10^0 to 10^{10}, and the installation position of the supports at two ends is set to be $\varepsilon_1 = \varepsilon_2^* = 0.06$.

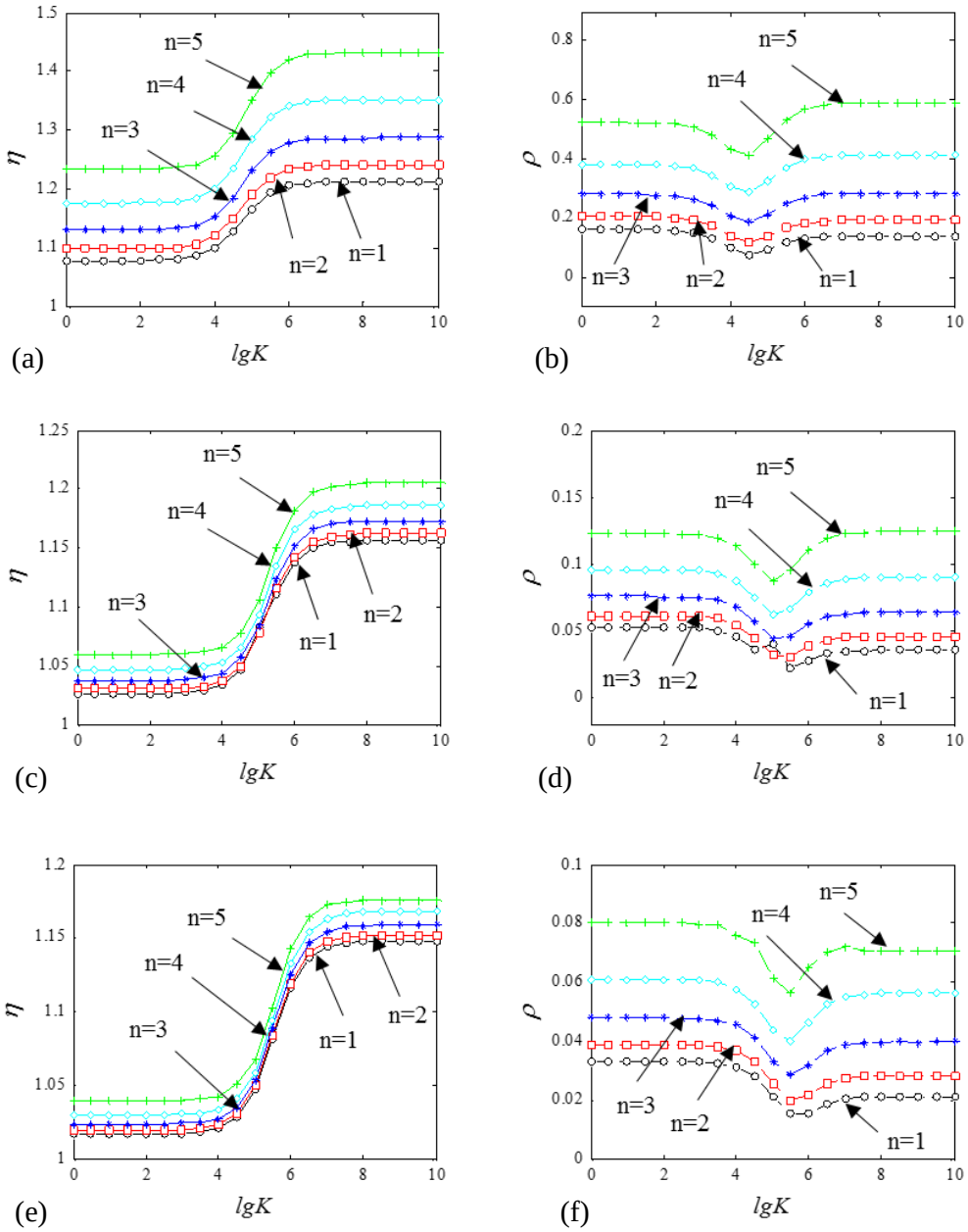

Fig. 7. Influence of mode order on frequency ratio and relative error between two models in the cases of (a) and (b): $\xi = 30$; (c) and (d): $\xi = 80$; (e) and (f): $\xi = 110$.

Table 1. Parameters of three typical cables

number	EI(MN·m^2)	m（kg/m）	T（kN）	L（m）	ξ
1	0.031524	12.107	500	15	59.74
2	0.031524	12.107	500	24	95.58
3	0.031524	12.107	500	30	119.48

289 The finite element analysis is first used to calculate the vibration frequencies of the cables
290 with two intermediate supports under different supporting stiffness. Then, the frequency values
291 are substituted into the formulas of Model 1 and Model 2 shown in section 2 to calculate the
292 tension force of the cable, respectively.

293 Fig. 8 shows the comparative results of the calculated tension force of (a) cable 1$^{\#}$, (c) cable
294 2$^{\#}$, and (e) cable 3$^{\#}$, and its relative error for (b) cable 1$^{\#}$, (d) cable 2$^{\#}$, and (f) cable 3$^{\#}$. Three
295 observations can be drawn from Fig. 8. First, in practical engineering, the acceptable threshold
296 for the estimation of cable force is generally set to be 5%. The relative error between the tension
297 force obtained from Model 1 and the accurate value falls in the range of 2%, which indicates that
298 Model 1 considering the flexural rigidity of the cable has very high identification accuracy, fully
299 meeting the requirement of practical engineering. Second, the relative error between the tension
300 force obtained from Model 2 and the accurate value is largely affected by the parameters of ξ
301 and K. The increase of ξ results in the decrease of the relative error. In particular when
302 ξ=95.58 for Cable 2 and ξ=119.48 for cable 3, the relative errors are smaller than 5% no matter
303 how K changes, which is identical to the conclusion obtained in section 4.1. Whereas for Cable
304 1$^{\#}$ with ξ=59.74, some relative errors are larger than 5%. Third and last, the support stiffness
305 K has a distinct effect on the relative error. For the three typical cables, there always exists a
306 special value, for instance $K=10^5$ for Cable 1$^{\#}$, leading to the smallest relative error. The

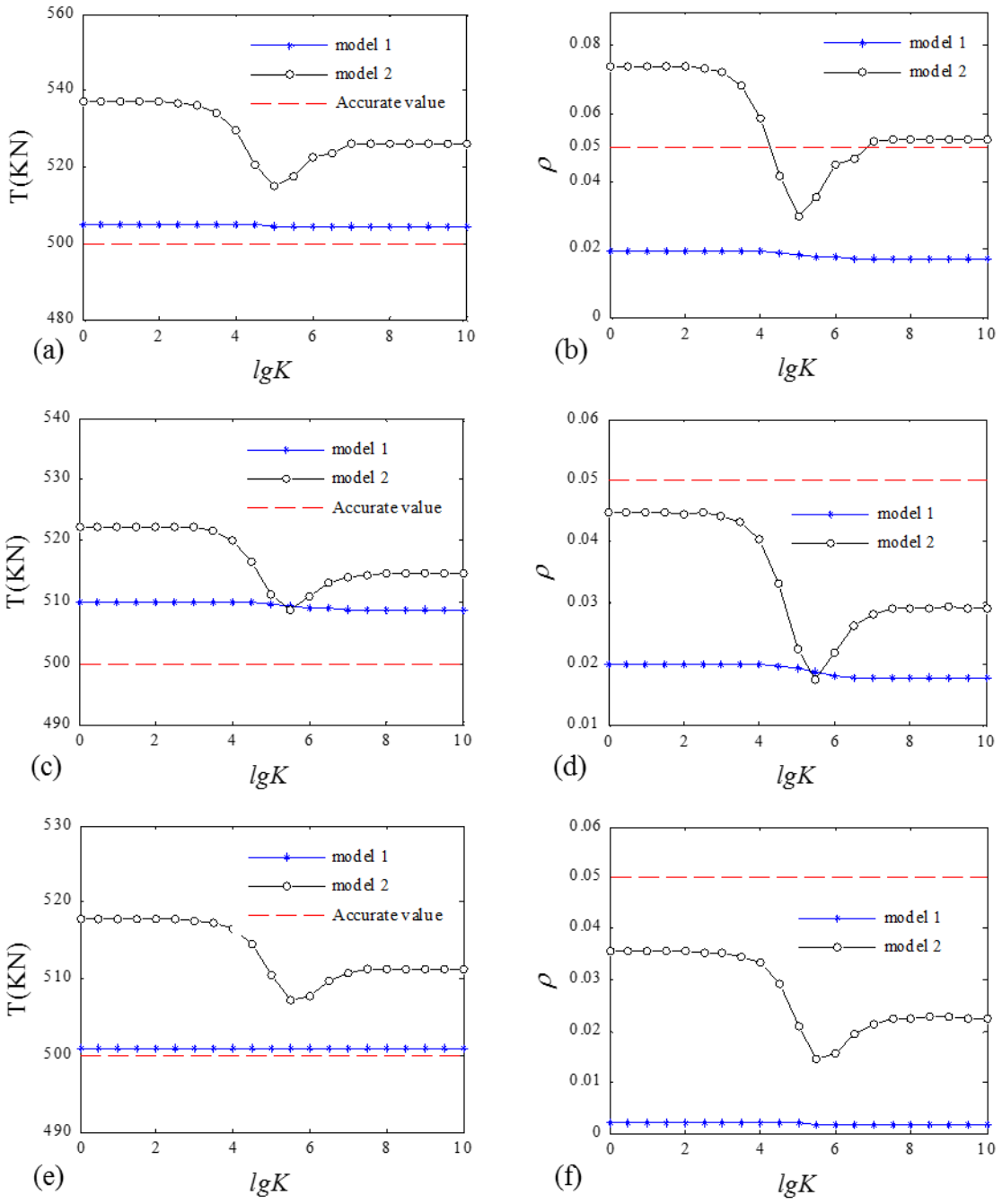

Fig. 8. Calculation of tension force value and its relative error distribution law for each model: (a) and (b): cable 1#; (c) and (d): cable 2#; (e) and (f): cable 3#

numerical study indicates that Model 2 is feasible for practical engineering at acceptable accuracy only at certain values of ξ.

6 Illustrative Examples

311 To verify the effectiveness and accuracy of the proposed Model 1 and Model 2 in estimation of
312 cable tension force, these models are investigated with two real-world arch bridges, Guitang River
313 Bridge located at Changsha, Hunan, P.R China and Sanan Yongjiang Bridge located at Nanning,
314 Guanxi. The ambient vibration measurement on hanger cables is collected to identify their
315 vibration frequencies, and further to estimate their tension forces by using Model 1 and Model 2.

316 *6.1 Case 1: A tied arch bridge*

317 As shown in Fig. 9, Guitang River Bridge is a down-supported tied arch bridge with a span length
318 of 84 *m*. The bridge has two arch ribs composed of steel box sections. Its deck is made from cast-
319 in-place prestressing concrete suspended from the arch by 14 pairs of hanger cables, each having
320 a distance of 5.0 *m* in longitudinal direction and post-tensioning along their length by longitudinal
321 prestressed tendons running either side of the deck. These tendons also act as ties for the arch to
322 resist the horizontal thrust within the structure.

323 The hanger cables have a standard tensile strength of 1,770 MPa. The compression-type
324 high-damping rubber (HDR) dampers are 150 *mm* high and 60 *mm* thick. Its modulus of elasticity
325 is 8.0 MPa. They are installed at the top anchorage zone of the hanger cables close to the arch ribs
326 and at the bottom of the tied deck. The supporting stiffness of the damper is $k = 9.19 \times 10^5$ N/m.

Fig. 9. View of Guitang River Bridge

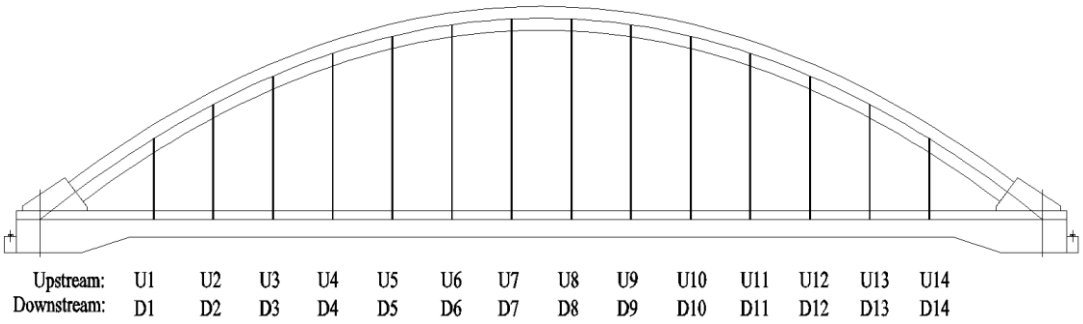

Fig. 10. Hanger cable arrangement of Guitang River Bridge

Fig. 10 shows the hanger cable arrangement of the bridge. The ambient vibration is measured on Cables U3~U12 at the upstream side and D3~D12 at the downstream side before and after the installation of the HDR dampers. The short cables U1, U2, U13, U14, D1, D2, D13, and D14 are not considered as their ambient vibration responses are weak. Table 2 presents the parameters and the measured fundamental frequencies of these cables. It is observed that the dimensionless parameter ξ is in the range of 31.58 to 44.90, which indicates that the cables appear to be very stiff. Note that, before the installation of dampers, the cable can be simply treated as a tensioned beam with two fixed ends. As such, the actual tension force of the cable can be estimated by solving a transcendental equation of the cable through an iterative method, assuming no change on the cable force after the installation of the dampers.

Fig. 11 shows the typical time history of measured acceleration for Cable U4 and its power spectrum. It is observed that the first four order modes can be clearly identified. As described in section 4.2, the first order mode generally exhibits the highest identification accuracy, hence in the study, only the fundamental frequency is considered for further estimation of the cable force.

Table 2. The basic parameters of the cable

Number		L (m)	m（Kg/m）	ε_1 (m/m)	ε_2^* (m/m)	f1 (Hz)	f2 (Hz)	ξ
	U3	13.251	35.6	0.083	0.187	8.567	9.710	31.62
	U4	15.251	35.6	0.072	0.163	7.606	8.453	37.61
	U5	16.754	35.6	0.066	0.148	6.453	7.210	38.59
	U6	17.758	35.6	0.062	0.140	6.224	6.802	42.03
Up	U7	18.259	35.6	0.060	0.136	6.224	6.968	44.61
stream	U8	18.259	35.6	0.060	0.136	6.137	6.723	43.93
	U9	17.758	35.6	0.062	0.140	6.220	6.968	42.00
	U10	16.754	35.6	0.066	0.148	6.594	7.446	39.50
	U11	15.251	35.6	0.072	0.163	7.511	8.608	37.13
	U12	13.251	35.6	0.083	0.187	8.645	10.023	31.93
	D3	13.251	35.6	0.083	0.187	8.556	9.987	31.58
	D4	15.251	35.6	0.072	0.163	7.569	8.492	37.45
	D5	16.754	35.6	0.066	0.148	6.555	7.417	39.24
	D6	17.758	35.6	0.062	0.140	6.113	6.662	41.26
Down	D7	18.259	35.6	0.060	0.136	6.102	6.846	43.78
stream	D8	18.259	35.6	0.060	0.136	6.268	7.024	44.90
	D9	17.758	35.6	0.062	0.140	6.167	6.839	41.61
	D10	16.754	35.6	0.066	0.148	6.433	6.905	38.47
	D11	15.251	35.6	0.072	0.163	7.484	8.695	36.99
	D12	13.251	35.6	0.083	0.187	8.613	10.149	31.80

Note: f1: the fundamental frequency of the cable before the installation of the damper.

f2: the fundamental frequency of the cable after the installation of the damper.

U: refers to the upstream cable.

D: refers to the downstream cable.

341 Fig. 12 displays the variation of the dimensionless parameter η before and after the

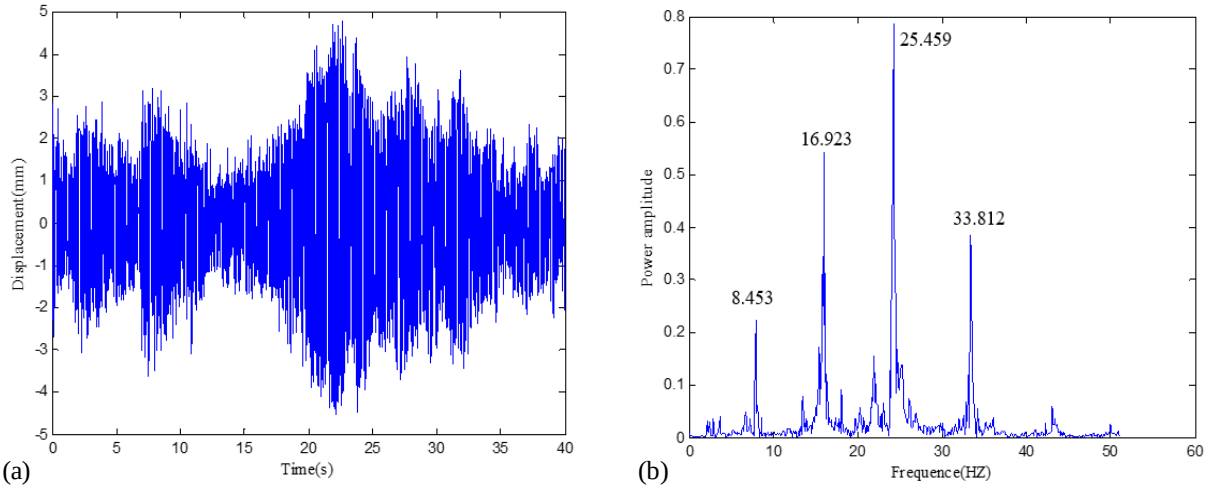

(a) (b)

Fig. 11. (a) Time history of accelerations and (b) power spectrum of Cable U4

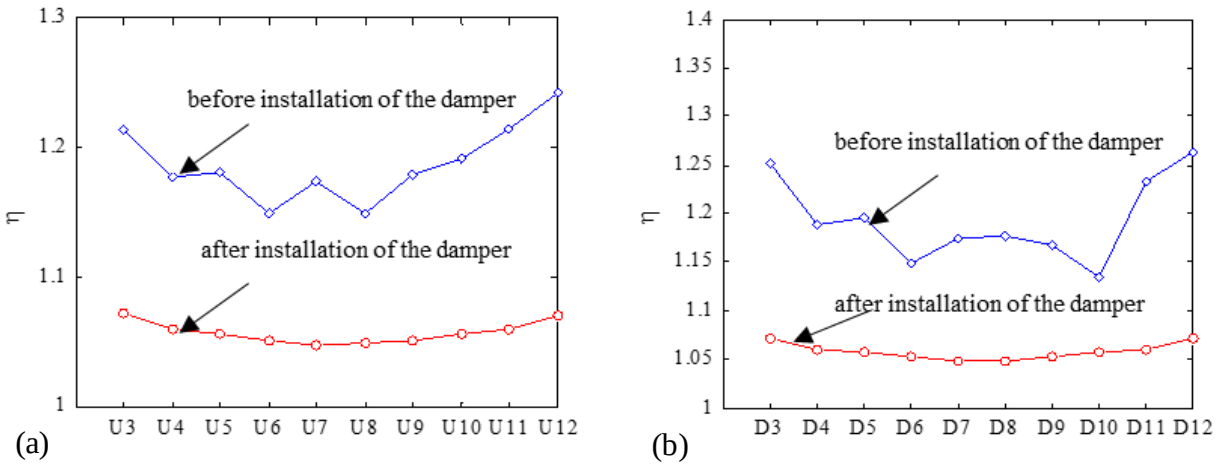

Fig. 12. The fundamental frequency of the cable before and after installation of dampers: (a) upstream cable and (b) downstream cable

installation of HDR dampers for the cables. It is observed that the parameter η changes significantly as the intermediate supports distinctly enhance the overall stiffness of the cable system. Fig. 13 indicates the comparison of the tension forces between the exact value obtained from the measurement results before the installation of dampers and that estimated via Model 1 and Model 2. The relative error is thus defined as

$$\rho' = \frac{T_i - T_b}{T_b} \tag{20}$$

where T_i $(i = 1, 2)$ are the tension forces calculated respectively according to Model 1 and Model 2 after the installation of HDR dampers and T_b is the exact value obtained from a tensioned beam model with two fixed ends before the installation of HDR dampers.

It is observed that the difference between the exact value and the estimated value via Model 1 is small (<1%) and relatively large (>5%) for Model 2. Moreover, for Model 2, it is also observed that the relative error decreases as the ξ value increases, which is consistent with the observation obtained in section 4.1. From the view of practical application, similarly when ξ is smaller than 90, it is better to estimate the cable force based on Model 1 so as to obtain acceptable identification accuracy.

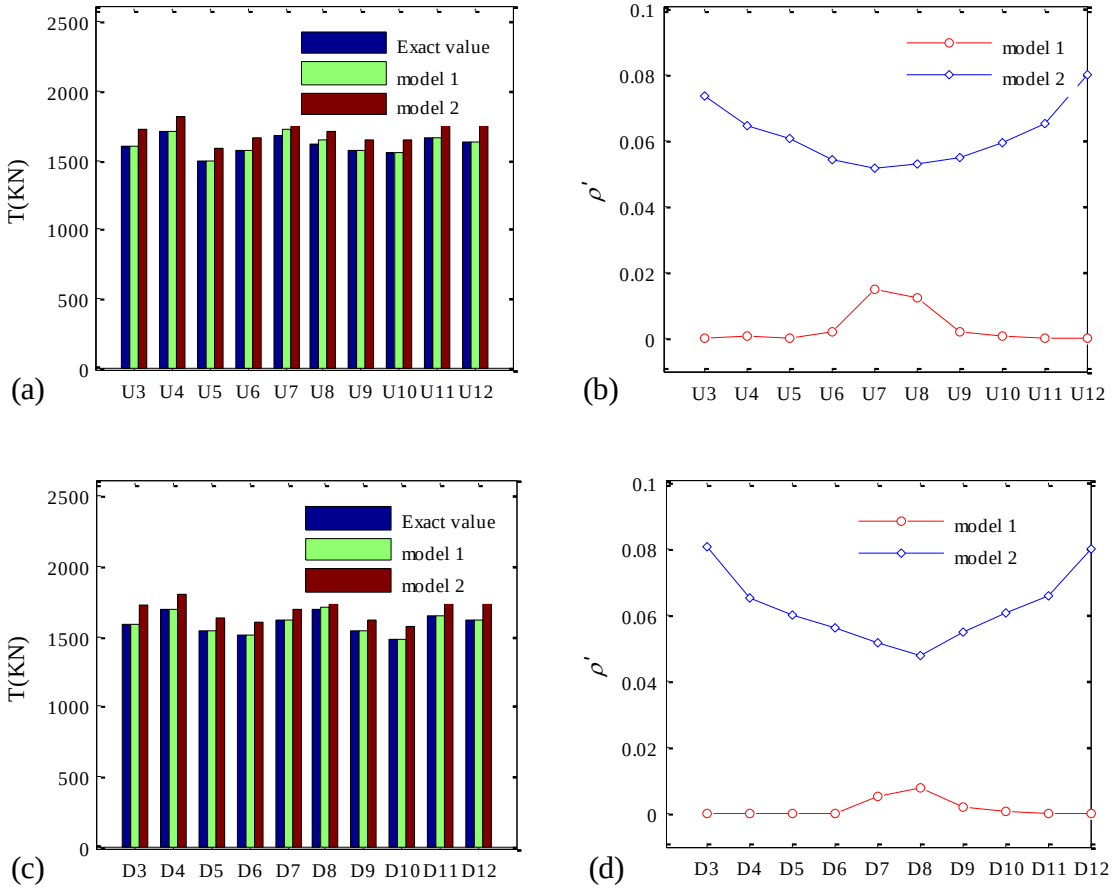

Fig. 13. Comparison of the calculated results of the two models with the exact values and the relative errors for: (a) and (b) upstream cables; (c) and (d) downstream cables

6.2 Case 2： Half-through arch bridge

As shown in Fig. 14, Sanan Yongjiang Bridge is a half-through concrete-filled steel tubular arch bridge with a main span of 270 *m*. The slab structure is composed of simply supported low-profile

Fig. 14. View of Sanan Yongjiang Bridge

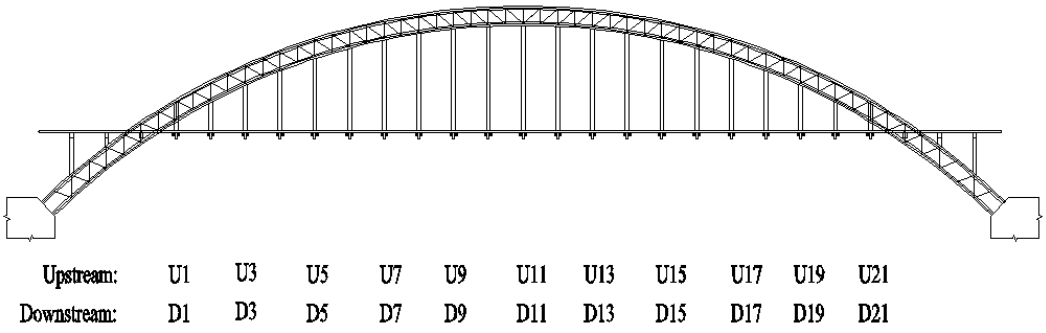

Fig. 15. Hanger cable arrangement of Sanan Yongjiang Bridge

T beams and directly supported by prestressed concrete transverse beams. The beam is suspended at two ends each by a pairs of hanger cables. The suspender system, as shown in Fig. 15, consists of 21 pairs of hanger cables with a distance of 10 *m* in longitudinal direction on each transverse side of the bridge, resulting in a total number of 84 hanger cables in the bridge. The HDR compression-type dampers with the height of 150 *mm*, the thickness of 45 *mm*, and the modulus of elasticity of 8 MPa are installed at both ends of the hanger cable. The supporting stiffness of the damper is $k = 2.32\times10^{6}$ N/m. Note that there is no force transducer at the anchorage zone of the hanger cable, thus, the actual tension force is not available for further comparative study. Since the arch bridge has no strictly defined longitudinal beam, the actual tension force of the hanger cable can be directly determined according to the weights of the transverse beams, the top low-profile T beams and the pavement system acted on the hanger cable within every two transverse beam.

The ambient vibration test is conducted to measure the tension forces of upstream hanger cables numbered as Cable U2-1, U2-2 to Cable U11-1, U11-2. The basic parameters of the cable are shown in Table 3. It is indicated that the value of dimensionless parameter ξ is in the range of 34.28 to 116.38, and the support position ε_1 and ε_2^* are respectively in the ranges of 0.035 (long cable) to 0.129 (short cable) and 0.027 (long cable) to 0.101 (short cable).

Table 3. The basic parameters of the cable

Number	L(m)	m/(Kg·m^{-1})	ε_1 (m/m)	ε_2^* (m/m)	Exact value (kN)	f/HZ	ξ
U2-1	8.86	20.5	0.129	0.101	1280	17.06	34.28
U2-2	9.49	20.5	0.121	0.094	1306	15.89	37.09
U3-1	13.9	20.5	0.082	0.064	1096	9.29	49.76
U3-2	14.45	20.5	0.079	0.062	1070	8.8	51.11
U4-1	18.33	20.5	0.062	0.049	1060	6.78	64.53
U4-2	18.82	20.5	0.061	0.048	1050	6.58	65.95
U5-1	22.16	20.5	0.052	0.040	1100	5.65	79.48
U5-2	22.58	20.5	0.051	0.040	1128	5.69	82.01
U6-1	25.4	20.5	0.045	0.035	1190	5.05	94.75
U6-2	25.74	20.5	0.044	0.035	1192	4.78	96.10
U7-1	28.05	20.5	0.041	0.032	1093	4.37	100.28
U7-2	28.32	20.5	0.040	0.032	1062	4.23	99.80
U8-1	30.11	20.5	0.038	0.030	1145	4.15	110.18
U8-2	30.31	20.5	0.038	0.030	1148	4.13	111.05
U9-1	31.58	20.5	0.036	0.028	1100	3.86	113.26
U9-2	31.72	20.5	0.036	0.028	1140	3.92	115.81
U10-1	32.48	20.5	0.035	0.028	1098	3.74	116.38
U10-2	32.55	20.5	0.035	0.027	1112	3.76	117.37
U11-1	32.8	20.5	0.035	0.027	1036	3.60	114.16
U11-2	32.8	20.5	0.035	0.027	1016	3.53	113.06

Fig. 16 shows the comparison of the tension forces between the exact values calculated from the weights acted on the hanger cable and those estimated via Model 1 and Model 2. It is observed that for Model 1, the relative errors of tension force for all hanger cables are within 3%, whereas for m2, the relative errors are within 7%. In particular, for Cables U2-1, U2-2 with $\xi < 40$, $\varepsilon_1 > 0.12$ and $\varepsilon_2^* > 0.09$, the relative error is about 1% for Model 1 and 6% for Model 2, which indicates that Model 1 considering the effect of flexural rigidity is capable of identifying the cable force with the higher accuracy. The accuracy from Model 2 is relatively small when directly estimating the tension force of the stiff hanger cable without considering its flexural rigidity. Furthermore, with the increase of ξ from 79.48 for Cable U5-1 to 113.06 for Cable U11-2, the difference between Model 1 and Model 2 decreases to an acceptable level, which demonstrates

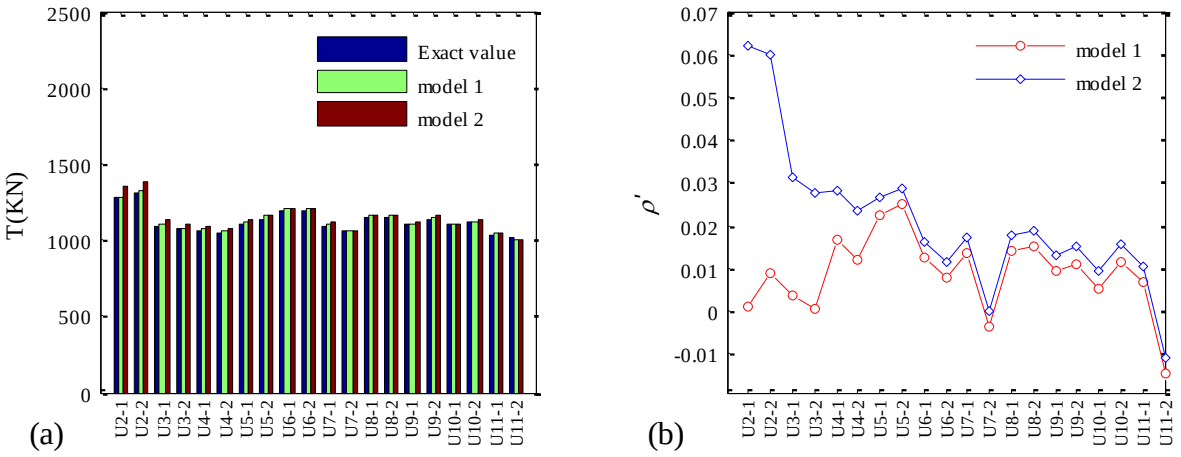

Fig. 16. Comparison of the calculated results of the two models with the exact values and the relative errors for: (a) and (b) upstream cables; (c) and (d) downstream cables

that in such cases Model 2 and Model 1 have the similar accuracy.

6. Conclusions

This paper proposes two analytic models to estimate the tension force of a cable with two intermediate supports from the measured frequencies. We derived an accurate model (Model 1) considering the flexural rigidity and a simple model (Model 2) without considering it. The effect of two intermediate supports on the identification accuracy of the cable tension force is analytically investigated via parametric analysis. The relative error is further analyzed to investigate the effects of non-dimensional parameters including damper location ε, support stiffness K, flexural rigidity ξ, and mode order of the cable. It is theoretically concluded that Model 2 provides an acceptable accuracy level at $\xi \geq 90$.

Numerical study about the effect of K and ξ on the identification accuracy of Model 1 and Model 2 indicates that the simplified Model 2 can be employed for practical engineering only at a certain range of ξ. Generally, in the case of $\xi \geq 90$, the relative error of the cable force obtained from Model 2 is in the range of 5%. Furthermore, field tests on the hanger cables of two

real-world arch bridges are conducted for further verification of two models. It is observed that Model 2 can be used in practical engineering when $\xi \geq 90$ in the case of slender cable, yielding the relative error of smaller than 5%. Whereas the complicate Model 1 can be applied to any cable system with two known intermediate support stiffness.

ACKNOWLEDGEMENTS

The authors gratefully acknowledge supports from the National Natural Science Fund of China (Grant Number: 51578227) and the Major Program of Science and Technology of Hunan Province (Grant Number: 2017SK1010).

References

1. H.M. Irvine, Cable structures, The MIT Press, Cambridge, Massachusetts, and London, England (1981).
2. E.D.S. Caetano, Cable vibrations in cable-stayed bridges, IABSE-AIPC-IVBH, Zurich, Switherland (2007).
3. H. Zui, T. Shinke, Y. Namita, Practical Formulas for Estimation of Cable Tension by Vibration Method, *J. Struct. Eng., ASCE,* **122** (1996) 651-656.
4. W.X. Ren, G. Chen, W.H. Hu, Empirical formulas to determine cable tension using fundamental frequency, *Struct. Eng. Mech.,* **20** (2005) 363-380.
5. Z. Fang, J.Q. Wang, Practical formula for cable tension estimation by vibration method, *J Bridge Eng., ASCE,* **17** (2012) 161-164.
6. M. J. Maurizi, P. M. Belles, General equation of frequencies for vibrating uniform one-span beams under compressive axial loads, *J. Sound Vib.,* **145** (1991) 345-347.
7. B.H. Kim, T. Park, Estimation of Cable Tension Force Using the Frequency-based System Identification

Method, *J. Sound Vib.,* **304** (2007) 660-676.

8. L. Ma, A highly precise frequency-based method for estimating the tension of an inclined cable with unknown boundary conditions, *J. Sound Vib.,* **409** (2017) 65-80.

9. S. Krenk, Vibrations of a taut cable with an external damper, *Int. J. Appl. Mech.,* **67** (2000) 772-776.

10. A. Nakamura, A. Kasuga, H. Arai, The effects of mechanical dampers on stay cables with high-damping rubber, *Constr Build. Mater.,* **12** (1998) 115-123.

11. H. Tabatabai, B. Mehrabi, Design of mechanical viscous dampers for stay cables, *J. Bridge Eng., ASCE,* **5** (2000) 114-123.

12. J. A. Main, and N. P. Jones. Free vibrations of taut cable with attached damper. I: Linear viscous damper. *J. Eng. Mech., ASCE,* **128** (2002) 1062-1071.

13. N. Hoang, Y. Fujino, Analytical study on bending effects in a stay cable with a damper, *J. Eng. Mech., ASCE,* **133** (2007) 1241-1246.

14. N. Hoang, Y. Fujino, Combined damping effect of two dampers on a stay cable, *J. Bridge Eng., ASCE,* **13** (2008) 299-303.

15. Z.H. Huang, P. J. Nicholas, Damping of taut-cable systems: Effects of linear elastic spring support, *J. Eng. Mech., ASCE,* **137** (2011) 512-518.

16. D.H. Dan, B. Xu, and Z.H. Chen. Universal characteristic frequency equation for cable transverse component system and its universal numerical solution, *J. Eng. Mech., ASCE,* **142** (2015) 04015105.

17. H.J. Zhou, X.G. Huang, X. Ning, J.W. He, L. M., Sun, F. Xing, Free vibration of a taut cable with a damper and a concentrated mass, *Struct. Control Hlth.,* **25** (2018) e2251.

18 M. Ghadiri, M. Kazemi, Nonlinear Vibration Analysis of a Cable Carrying Moving Mass-Spring-Damper, *Int. J. Struct. Stab. Dyn.,* **18** (2018) 1850030.

19. P. Zhou, M. Liu, H. Xiao, et al. Feasibility of using a negative stiffness damper to two interconnected Stay Cables for damping enhancement, *Int. J. Struct. Stab. Dyn.,* **19** (2019) 1950058.

20. M.A. Ceballons, C.A. Prato, Determination of the axial force on stay cables accounting for their bending stiffness and rotational end restraints by free vibration tests, *J. Sound Vib.,* **317** (2008) 127-141.

21. C.C. Chen, W.H. Wu, M.R. Leu, G. Lai, Tension determination of stay cable or external tendon with complicated constraints using multiple vibration measurements, *Measurement.,* **86** (2016) 182-195.

22. C.C. Chen, W.H. Wu, S.Y. Chen. G.L. Lai, A novel tension estimation approach for elastic cables by elimination of complex boundary condition effects employing mode shape functions, *Eng. Struct.,* **166** (2018) 152–166.

23. B.F. Yan, J.Y. Yu, M. Soliman, Estimation of cable tension force independent of complex boundary conditions, *J. Eng. Mech., ASCE,* **141** (2014) 06014015.

24. B.F. Yan, W.B. Chen, J.Y. Yu, X.M. Jiang, Mode shape-aided tension force estimation of cable with arbitrary boundary conditions, *J. Sound Vib.,* **440** (2019) 315-331

25. D.H. Dan, Y.Y Chen, X. F. Yan, Determination of cable force based on the corrected numerical solution of cable vibration frequency equations, *Struct. Eng. Mech.,* **50** (2014): 37-52